Contents lists available at ScienceDirect

Geoderma

journal homepage: www.elsevier.com/locate/geoderma

Tracking biological and mechanical subsoil amelioration via multi-coil electromagnetic induction

Aaron Sobbe [a], Jessica Schmäck [b], Cosimo Brogi [b], Anja Klotzsche [b], Lutz Weihermüller [b], Harry Vereecken [b], Enzo Rizzo [a], Jan van der Kruk [b,*]

[a] Department of Physics and Earth Sciences, Via G. Saragat, 1, 44121, University of Ferrara, Italy
[b] Agrosphere Institute IBG-3, Forschungszentrum Jülich GmbH, 52425 Jülich, Germany

ARTICLE INFO

Handling Editor: Dr. H. Neely

Keywords:
Electromagnetic induction
Apparent electrical conductivity
Soil memory
Lucerne (*Medicago sativa L.*)
Bio-drilling
Subsoil management
Time-lapse monitoring

ABSTRACT

Subsoil compaction limits root growth and water uptake, often amplifying crop stress during drought. Biological "bio-drilling" with deep-rooting plants is a sustainable alternative to mechanical tillage, creating stable biopores and improving soil structure and water infiltration, but assessing its long-term effectiveness remains challenging. This study evaluates the use of a multi-coil electromagnetic induction (EMI) system to monitor subsoil responses to various loosening strategies, including biological treatments (Lucerne and Ryegrass mixture) and mechanical deep loosening with or without compost incorporation. EMI surveys prior to the experiment revealed inherent soil heterogeneity, emphasizing the importance of baseline mapping for robust experimental design. To isolate management-induced signatures, an innovative data processing workflow was implemented to effectively disentangle anthropogenic structural legacies from the dominant pedological "soil memory" (i.e., inherent natural soil heterogeneity). Time-lapse surveys tracked treatment effects over subsequent cropping seasons. Complementary EMI point measurements showed a distinct negative trend in apparent electrical conductivity (*ECa*), consistent with soil drying associated with crop development and root water uptake. This suggests that biological and mechanical amelioration may leave lasting structural signatures in the subsoil that modify water accessibility and hydraulic connectivity, ultimately enhancing the crop's ability to exploit deep water reserves. By combining spatial and temporal monitoring, EMI provides a powerful tool to link soil structural changes to crop water dynamics and resource use efficiency. This work shows how non-invasive geophysical methods can reveal subtle but ecologically meaningful responses in the soil-root continuum under real cropping conditions and supports the potential of bio-drilling to reduce subsoil compaction.

1. Introduction

The subsoil represents a major reservoir of water and nutrients, storing up to 50% of total soil nitrogen and more than half of plant-available water in agricultural systems (Kautz et al., 2013a; Ning et al., 2022). In many temperate agroecosystems, however, access to these resources is restricted by dense subsoil layers resulting from pedogenesis and agricultural traffic, which increase soil strength and limit root penetration (Hamza and Anderson, 2005; Keller et al., 2013). As climate change is expected to intensify drought occurrence and water scarcity (Berg and Sheffield, 2018), improving crop access to deep soil resources is increasingly critical for yield stability and resource-use efficiency (Seidel et al., 2019; Gocke et al., 2021). To overcome subsoil constraints, either mechanical or biological amelioration approaches have been proposed (Ning et al., 2022). Mechanical interventions, such as deep loosening combined with organic amendments, aim to disrupt compacted layers and stabilize the resulting pore system (Schneider and Don, 2019; Arslan et al., 2026). Biological approaches rely on deep-rooting species such as Lucerne (*Medicago sativa L.*), whose roots can penetrate dense horizons and create vertically connected biopores, facilitating the rooting of subsequent crops (Kautz et al., 2013a; Han et al., 2015). These biologically generated macropore networks may improve subsoil aeration, water movement, and access to deep soil resources, thereby contributing to enhanced drought resilience and crop productivity (Kirkegaard et al., 2007; Gaiser et al., 2012; Seidel et al., 2019).

Despite their recognized potential, evaluating the long-term effectiveness of subsoil amelioration remains challenging. Structural modifications induced by management are embedded within the highly heterogeneous soil–plant-atmosphere continuum, where changes in soil architecture, root development, water redistribution, and plant uptake interact across multiple spatial and temporal scales (Passioura, 2002; Vereecken et al., 2016). As a result, novel management-induced responses are often difficult to separate from pre-existing patterns in soil variability generated by soil formation processes and historical agricultural practices, particularly in long-term experiments. This persistence can be interpreted as a manifestation of "soil memory", defined as the capacity of soils to retain and express signatures of past environmental conditions and management actions through time (Rahmati et al., 2024). In agricultural fields, soil memory is reflected in the temporal stability of spatial patterns associated with texture, structure, and hydrological functioning (Johnson et al., 2005). At the same time, management interventions may create their own structural legacies, for example through the formation of stable biopore networks or persistent modifications of pore connectivity. These anthropogenic imprints may persist for years following subsoil amelioration interventions and become embedded within the broader soil memory of the site, making their detection and attribution particularly challenging. Distinguishing these anthropogenic signatures from the underlying pedological background is therefore essential for understanding the long-term impact of subsoil management.

Traditional soil sampling and coring approaches provide valuable information but remain limited by their destructive nature, restricted sampling volume, and poor spatial coverage (Cimpoiaşu et al., 2020). Furthermore, because of the inherent difficulty of accessing the subsoil, this remains largely a "black box" in most agricultural monitoring and soil health policies, which typically focus on the more accessible topsoil layers (Rumpel et al., 2012; Amelung et al., 2020). In contrast, hydro- and agrogeophysical methods offer non-invasive monitoring of subsurface processes at field scale (Binley et al., 2015). These techniques have become essential for characterizing the soil-root continuum across different spatial and temporal scales (Romero-Ruiz et al., 2018; Garré et al., 2021). For example, Electrical Resistivity Tomography (ERT) is frequently employed to visualize 2D and 3D soil water dynamics and root-induced depletion zones (Garré et al., 2011; Cassiani et al., 2015), while Ground Penetrating Radar (GPR) has proven effective in mapping soil horizons and identifying localized compaction layers (Grote et al., 2010; Kaufmann et al., 2020a; Sobbe et al., 2025). In this context, modern multi-coil Electromagnetic Induction (EMI) systems offer a distinct advantage by enabling the rapid and simultaneous mapping of the soil root zone without the need for direct ground contact, facilitating large-scale applications (von Hebel et al., 2014; Frederiksen et al., 2017; Brogi et al., 2019; Brogi et al., 2021; Dogar et al., 2025). Moreover, EMI is increasingly used to monitor the long-term impact of agricultural management (Kaufmann et al., 2025), characterize site variability, and monitor temporal dynamics (Martini et al., 2017; Kaufmann et al., 2020b). EMI measures the apparent Electrical Conductivity (*ECa*) of the ground, which integrates information on soil water content, texture, clay content, pore connectivity, and root-induced water depletion (Corwin and Lesch, 2005; Heil and Schmidhalter, 2017; Ni et al., 2019; Brown et al., 2021; Schmäck et al., 2022). Consequently, EMI provides a unique opportunity to monitor how structural and functional soil properties evolve through time and to investigate the interaction between soil architecture and crop water uptake (Stadler et al., 2015; Martini et al., 2017; von Hebel et al., 2018; Brogi et al., 2020; Cimpoiaşu et al., 2020; Quiros-Vargas et al, 2026). Rather than directly imaging structural features, EMI primarily captures their integrated geophysical response through changes in soil water redistribution, root development, and plant water uptake. However, the interpretation of EMI data in long-term field experiments remains complicated as treatment-induced soil changes are often much smaller than the background variability generated by inherent pedological heterogeneity (Jung et al., 2005; Robinson et al., 2008). Unfortunately, methods that can separate persistent soil memory from management-induced signatures remain limited, and it is still unclear how subsoil amelioration legacies evolve and influence field-scale root water uptake dynamics.

Within the "Soil^3 – Sustainable Subsoil Management" experiment at the Campus Klein-Altendorf CF2 research station (Bonn, Germany), we used multi-coil electromagnetic induction (EMI) to investigate the long-term impacts of biological (Lucerne vs. Ryegrass) and mechanical (deep loosening ± compost) subsoil management. Combining four years of field-scale bare soil EMI surveys with repeated cropped point-scale measurements, we developed a spatio-temporal analysis framework designed to distinguish persistent pedological background patterns from management-induced geophysical signatures and to evaluate their evolution through time.

Specifically, the objectives of this study were to:

i) quantify the spatial magnitude, persistence, and depth dependence of management effects on apparent electrical conductivity (*ECa*);
ii) evaluate the ability of a combined Mean Subtraction and Background Subtraction (MS-BS) approach to separate treatment-induced responses from the underlying soil memory of the experimental site;
iii) investigate the relationship between temporal *ECa* dynamics and crop water uptake under contrasting biological and mechanical subsoil amelioration strategies.

By focusing on relative spatio-temporal changes rather than absolute conductivity values, this study explores how EMI can be used to identify and track long-term structural legacies of subsoil management and their functional implications for soil water exploitation under field conditions.

2. Materials and methods

2.1. Field site

This study was conducted at the University of Bonn's Experimental Station "Campus Klein-Altendorf" in Rheinbach, Germany (50°38'5.71" N, 6°58'37.24" E), at elevations between 163 and 166 m a.s.l. The field site hosts the Central Field Experiment 2 (CF2), one of the main experimental platforms established during the second phase of the Soil3 project (https://doi.org/10.20387/BonaRes-BSZH-QBKN). CF2 was designed to investigate how biological and mechanical subsoil management strategies interact and complement each other in shaping soil functioning, crop performance, and environmental outcomes. The experimental area is located on agricultural land affected by a compacted subsoil layer that limits deep rooting and reduces access to water stored below 60–80 cm depth. The site consists of replicated plots arranged to permit controlled management operations, the installation of sensors, and repeated non-invasive geophysical monitoring. The local climate is temperate and humid, with long-term averages of 9.6 °C mean annual temperature, 603 mm annual precipitation, and a marked summer water deficit of approximately −640 mm (Uhlig et al., 2023). The soil is classified as a Haplic Luvisol (hypereutric, siltic) developed from loess (IUSS Working Group WRB, 2015), featuring a silty clay loam texture and a clay-illuviated Bt horizon between roughly 45 and 95 cm, which reduces porosity and increases penetration resistance (Barej et al., 2014; Arslan et al., 2026). According to Barej et al. (2014), the profile exhibits increasing bulk density with depth (from ~ 1.29 to ~ 1.52 g/cm^3) and very low $CaCO_3$ contents in the upper 1.27 m, with a sharp increase in the deeper loess layer. Their work also reports strong vertical gradients in phosphorus fractions and organic matter. Further information on the soil's physical and chemical characteristics is provided in Barej et al. (2014).

* Corresponding author.
E-mail addresses: aaron.sobbe@unife.it (A. Sobbe), a.klotzsche@fz-juelich.de (A. Klotzsche), j.van.der.kruk@fz-juelich.de (J. van der Kruk).

https://doi.org/10.1016/j.geoderma.2026.118001
Received 28 April 2026; Received in revised form 20 July 2026; Accepted 17 August 2026
Available online 29 August 2026
0016-7061/© 2026 The Author(s). Published by Elsevier B.V. This is an open access article under the CC BY license (http://creativecommons.org/licenses/by/4.0/).

2.2. Experimental design and subsoil management

The experiment followed a four-year sequence (2016–2020) and aimed to evaluate the effects of biological and mechanical subsoil management on soil properties and crop performance within the CF2 platform. The experimental layout consisted of a factorial combination of biological pre-conditioning and mechanical subsoil treatments distributed across 40 replicated plots of approximately 18 × 12 m, separated by ~ 3 m inter-plot corridors to allow machinery access, covering an overall area of about 2 ha (Fig. 1). The plots were arranged in a fully randomized layout prior to any soil characterization. In late 2016, Lucerne (*Medicago sativa* L., indicated by *luc*) and a Ryegrass mixture (*Lolium perenne*, indicated by *rye*) were established on separate plots as contrasting biological pre-conditioning treatments and maintained for two consecutive growing seasons (spring 2017 to summer 2018). While Lucerne was selected to promote bio-drilling through the development of deep taproots and stable biopore networks, Ryegrass served as a shallow-rooted control to assess the influence of contrasting root architectures on subsoil pore development. Following the two growing seasons, both pre-crops were terminated by mulching to allow root decomposition and the subsequent establishment of the experimental cropping sequence. In October 2018, mechanical subsoil management was implemented using a specialized subsoiler designed to create 30-cm-wide slots at 30–60 cm depth with 70 cm spacing while avoiding topsoil-subsoil mixing (Schmittmann et al., 2021). Besides the untreated reference (Control), two mechanical treatments were applied: deep loosening (DL) and deep loosening combined with the incorporation of 3 kg m^{-2} of stabilized biowaste compost (DLB), consisting of grass clippings, wheat straw, and manure, into the 30–45 cm layer (Schmittmann et al., 2021; Uhlig et al., 2023). The compost was thermally treated prior to incorporation to eliminate pathogens and weed seeds. This strategy was intended to physically stabilize the loosened slots while improving deep nutrient and water availability (Arslan et al., 2026; Uhlig et al., 2023). The factorial combination of the two biological (*luc* or *rye*) and three mechanical (Control, DL, or DLB) treatments resulted in six management strategies: Control.luc, DL.luc, DLB.luc, Control.rye, DL.rye, and DLB.rye. The randomized allocation across the 40 plots resulted in six replicates for Control.luc and DLB.rye, and seven replicates for the remaining four treatments. The subsequent cropping sequence consisted of spring wheat (2019) followed by spring barley (2020), allowing crop performance to be evaluated under contrasting subsoil conditions.

2.3. EMI data collection

To characterize the spatial and temporal impact of the different subsoil treatments, a multi-year monitoring strategy based on EMI was implemented (Fig. 2). The sequence began with a survey on 11th August 2016 to characterize the initial field-scale soil conditions and inherent heterogeneity. Following the subsoil manipulations in 2018, additional field-scale surveys were conducted to track the evolution of soil structure and hydrological status: on 7th February 2019 on the bare soil (post-amelioration but prior to cropping), and on 15th October 2019 and 8th October 2020 following the harvest of the respective summer crops.

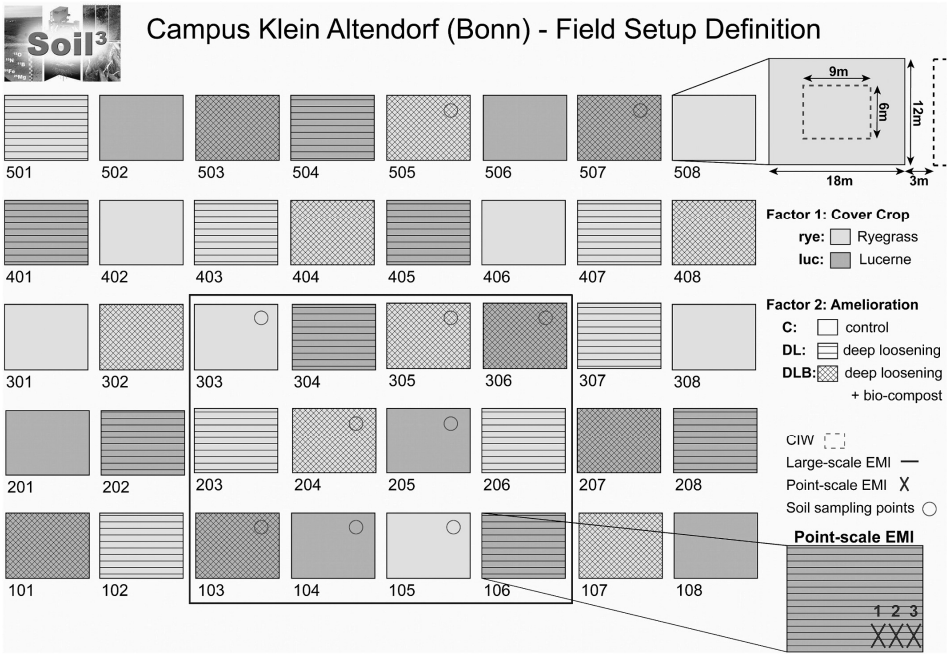


Fig. 1. Schematic representation of the agricultural site studied between 2016 and 2020 as part of the Soil[3] project at the experimental station of the University of Bonn, Campus Klein-Altendorf, Rheinbach, Germany (50°38′5.71″N, 6°58′37.24″E), showing the organization and distribution of cover crops and amelioration practices applied on the site. The blue rectangle identifies the area where the point-scale EMI measurements were carried out. CIW: centred internal window.

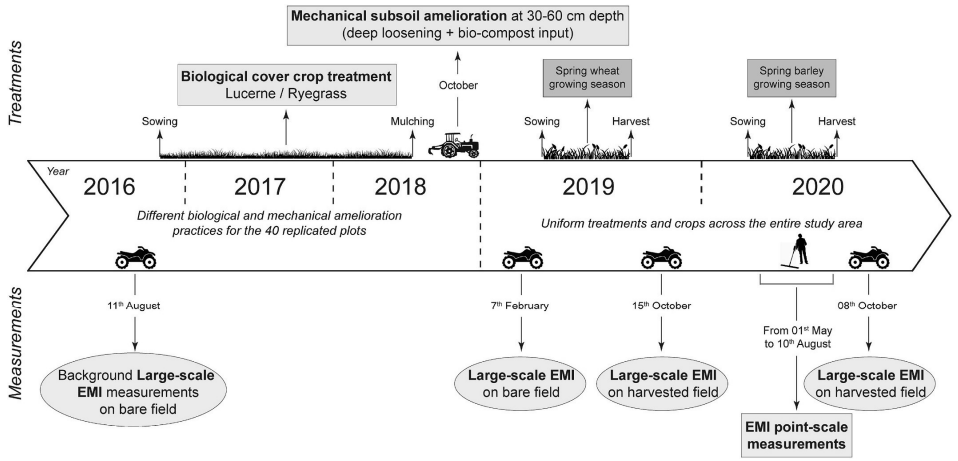


Fig. 2. Schematic experimental timeline of agricultural management and EMI measurement campaigns conducted between 2016 and 2020 at the CF2 site. The top section details the biological pre-conditioning (Lucerne and Ryegrass cover crops) and the mechanical subsoil amelioration (deep loosening and biowaste incorporation at 30–60 cm depth performed in October 2018). The central arrow illustrates the transition from the diverse treatment phase (2016–2018) to the uniform cropping phase with spring wheat (2019) and spring barley (2020) across the 40 replicated plots. The bottom section specifies the timing of large-scale EMI surveys (background, bare soil, and post-harvest) and the high-frequency point-scale EMI monitoring carried out during the 2020 growing season.

During the 2020 barley growing season, these bare soil large scale mappings were complemented by high-frequency point-scale cropped EMI measurements to capture the fine-scale temporal dynamics of within-plot water extraction of the crops.

Subsurface apparent electrical conductivity (*ECa*) was mapped using multi-coil frequency-domain EMI. The systems operated under low induction number conditions (Keller and Frischknecht, 1966; Ward and Hohmann, 1987). Traditionally, *ECa* values are derived from the ratio of the secondary to the primary magnetic field based on the linear approximation proposed by McNeill (1980). However, it is recognized that this linear relationship can introduce systematic errors, particularly for larger coil separations and in more conductive soils (von Hebel et al., 2019). Although, von Hebel et al. (2019) provided more quantitative and accurate conductivity estimates, this study focuses on relative spatio-temporal dynamics and signatures derived from inherent soil properties (i.e., the unmanaged soil background). Therefore, the standard *ECa* output was considered as a robust proxy for the comparative analysis of management-induced patterns. The depth of investigation (DOI) and the vertical sensitivity of the signal are governed by the inter-coil spacing and orientation. Following McNeill (1980), the DOI is defined as 0.75 and 1.5 times the coil separation for Vertical Coplanar (VCP) and Horizontal Coplanar (HCP) configurations, respectively. This DOI indicates the depth range where approximately 70% of the cumulative sensitivity is concentrated; conversely, materials located below the DOI contribute the remaining 30% to the measured *ECa* values (von Hebel et al., 2018). In this study, we utilized both VCP and HCP configurations. While VCP provides maximum sensitivity to near-surface layers, HCP offers greater DOI and peak sensitivity at deeper horizons (approximately 0.4 times the coil separation), making it more suitable for monitoring subsoil management effects (McNeill, 1980; von Hebel et al., 2014).

2.3.1. Large-scale EMI measurements

Large-scale EMI measurements were carried out to capture the spatial and temporal variability of *ECa* across the entire experimental field. Surveys were performed on four dates: 11th August 2016 (background bare soil), 7th February 2019 (post-amelioration bare soil), 15th October 2019, and 8th October 2020 (bare soil after harvest) (Fig. 2). Two EMI instruments developed by GF Instruments (Brno, Czech Republic) were operated simultaneously: (i) a CMD Mini-Explorer with three receiver coils, providing inter-coil spacings (*s*) of 32, 71, and 118 cm for the VCP configuration, and (ii) a custom-built CMD Mini-Explorer Special Edition with six coils featuring *s* values of 35, 50, 71, 97, 135, and 180 cm for the HCP configuration (Brogi, 2019), allowing concurrent acquisition of both VCP and HCP measurements at 30 and 25 kHz, respectively. The instruments were mounted on two non-conductive plastic sleds towed by an ATV at 5–7 km/h, with DGPS units (Trimble Inc., Sunnyvale, USA) installed on each sled to ensure precise spatial referencing. Measurements were collected continuously across the entire field CF2 (Fig. 1), which was free of vegetation and obstacles during all survey campaigns.

2.3.2. Point-scale EMI measurements

In addition to the field-scale EMI surveys, repeated point-scale EMI measurements were conducted during the 2020 growing season. These measurements were designed as a high-frequency monitoring component to complement the field-scale surveys and to investigate treatment-specific temporal *ECa* dynamics during crop development. Measurements were performed at ten dates between May and August during the 2020 barley growing season (sown on 25th March and harvested in mid-August) to characterise within-plot *ECa* variability in a field area previously identified as homogeneous, with the aim of assessing the impact of different soil management treatments and crop growth dynamics on *ECa* values over time. Measurements were conducted in twelve plots (blue rectangle in Fig. 1) at three fixed positions per plot (blue crosses 1–3 in Fig. 1). These measurement positions were intentionally located 1 m inside the southeastern plot margins rather than in the plot center. These measurement positions were intentionally located 1 m inside the southeastern plot margins rather than in the plot center to avoid potential boundary effects. Furthermore, these repeated point-scale

measurements serve as a representative bridge for validating the field-scale EMI observations and for evaluating the correlations with soil water contents. In these measurements, the CMD Mini-Explorer Special Edition was employed in VCP mode (see Table 1). At each location, three consecutive ~ 60 s measurements (≈300 readings recorded at 0.2 s intervals) were collected and averaged, resulting in 36 spatially referenced mean *ECa* values per survey date. The measurement setup was standardised across all dates: the coil assembly was placed 1 m inside the field and aligned North-South (perpendicular to the soil amelioration lines), while the console and operator were located at least 3 m away to avoid any electromagnetic perturbations. No calibration measurements were taken, as the primary objective was to analyse the relative differences among treatments and their temporal evolution rather than absolute *ECa* values. It is acknowledged that the absence of absolute calibration may introduce some degree of uncertainty when interpreting *ECa* in terms of exact volumetric soil water content or specific structural parameters. However, by maintaining a standardized measurement protocol and focusing on relative spatio-temporal dynamics through the MS & BS workflow, the geoelectromagnetic signatures remain a robust proxy for the functional response and structural legacies of the different subsoil treatments.

2.3.3. Signal contribution and treatment sensitivity

To quantify the contribution of specific subsurface intervals to the measured *ECa* signal, the cumulative response function $R(z)$ was used (McNeill 1980). This function, derived by integrating the relative sensitivity from a normalized depth z ($z = \text{depth}/s$) to infinity, describes the total contribution of the soil below depth z. For the HCP configuration (vertical dipoles), the cumulative response is defined as

$$R_{HCP}(z) = \frac{1}{\sqrt{4z^2 + 1}} \tag{1}$$

Conversely, for the VCP configuration (horizontal dipoles), it is expressed as

$$R_{VCP}(z) = \sqrt{4z^2 + 1} - 2z \tag{2}$$

These formulations allow for the calculation of the theoretical signal contribution $C(z_{top}, z_{bot})$ from any specific soil layer bounded by normalized depths z_{top} and z_{bot} by computing the difference

$$C(z_{top}, z_{bot}) = R(z_{top}) - R(z_{bot}) \tag{3}$$

2.4. Soil sampling and soil analysis

To complement the non-invasive geophysical EMI surveys, undisturbed soil samples were collected on June 29th, 2020, in correspondence of the 6th day of point-scale measurements, during the spring barley growing season. At the time of sampling, the crop had reached a height of 70 cm and was entering the early stages of senescence, characterized by the initial yellowing of the canopy observed on the field. Sampling was conducted across ten representative plots, paired based on treatment replicates as follows: 104–205 (Control.luc), 103–306 (DLB.luc), 105–303 (Control.rye), and 204–305 (DLB.rye). In addition, plots 505 and 507 were included to provide further sampling for the DLB.rye and DLB.luc treatments, respectively (Fig. 1). To minimize soil disturbance while ensuring high-quality sample recovery, soil cores were extracted using 250 cm^3 rings from the profile walls of existing 1.1 m deep trenches. These walls were extended laterally by approximately 20 cm to access fresh, undisturbed soil sections. The sampling design was specifically tailored to account for the subsoil management treatments. In the Control.rye and Control.luc plots, samples were collected at three depths: 15 cm (plow layer), 40 cm (designed amelioration depth), and 70 cm (below the management influence). In the plots DLB.rye and DLB.luc, the sampling targeted the induced structural heterogeneity: undisturbed samples were extracted directly from the compost stripes (35–45 cm depth) and from the loosened soil layer immediately above them (15–30 cm). For plots 505 and 507, a higher-resolution sampling scheme was implemented, including additional lateral samples at 15, 40, and 70 cm to characterize the within-plot spatial variability relative to the ameliorated zones. The collected samples were analysed for key physical and hydraulic properties to provide ground-truth data for the *ECa* measurements. Laboratory analyses included the determination of bulk density and soil water retention. The plant available water was calculated considering three different pressure heads for field capacity (FC): −100 cm, −200 cm, and −250 cm. The permanent wilting point was set at −15,000 cm (pF 4.2). For statistical analysis and data interpretation, samples were categorized into functional soil types based on their management and position: reference/undisturbed soil (Control.rye, Control.luc, DLB.rye, DLB.luc), loosened soil above the tillage slots (DLB.rye-DL, DLB.luc −DL), and the biowaste-enriched zone (DLB.rye-B, DLB.luc-B).

Table 1
Depth of investigation (DOI's) of the horizontal coplanar (HCP) and vertical coplanar (VCP) EMI configurations and the expected signal contribution originating from the 30–60 cm depth range.

			Signal Contribution from 30-60 cm [%]		
	DOI [m]		Mini-Expl.	Mini-Expl. Special Edition	
Coil Spacing [m]	VCP	HCP	VCP	VCP	HCP
0.32	0–0.24	–	11.9	–	–
0.35	0–0.26	0–0.52	–	12.8	22.4
0.50	0–0.38	0–0.75	–	16.2	25.6
0.71	0–0.53	0–1.06	19.1	19.1	25.5
0.97	0–0.73	0–1.46	–	20.4	22.2
1.18	0–0.89	–	20.4	–	–
1.35	0–1.01	0–2.03	–	20.1	16.7
1.80	0–1.35	0–2.70	–	18.6	11.7

2.5. Data processing

2.5.1. Bare field large-scale measurements data processing from 2016 to 2020

All large-scale EMI datasets were filtered to remove unrealistic values and outliers by using: (i) min–max threshold filtering to remove out-of-range measurements; (ii) histogram-based filtering to eliminate distributional outliers as suggested by von Hebel et al. (2014); (iii) maximum-variability filtering to suppress high-frequency, acquisition-related artefacts; and (iv) a moving-window mean filter to attenuate local noise. Then, measurements were converted to the UTM Zone 32 North reference system and interpolated onto a unified 0.5 m regular grid using a nearest neighbour algorithm. The grid extent was defined as the maximal common spatial domain shared by all surveys, with fixed bottom-left and top-right coordinates to ensure geometric congruence across acquisition dates and coil configurations. Prior to interpolation, each large-scale measurement dataset underwent a multistage quality-control and denoising procedure. The August 2016 dataset exhibited systematic horizontal streaking due to suboptimal sled geometry during acquisition. A supplementary column-wise smoothing filter was therefore applied to mitigate this directional artefact. Rectangular experimental plots were georeferenced by acquiring the GPS coordinates of their centroids. A centred internal window of 9 × 6 m (Fig. 1) centred on each plot was used as it represented the largest area that remained unaffected by boundary effects zones influenced by machinery-induced soil compaction. These rectangle geometries were overlaid onto the *ECa* maps and visualized using colour codes corresponding to the specific soil manipulation applied in each plot. It should be noted that, for the present study no calibration of the EMI data was performed using independent geoelectrical measurements, such as ERT or Vertical Electrical Sounding. Consequently, no data inversion was carried out to retrieve quantitative depth-specific electrical conductivity values. Instead, the analysis remains focused on the qualitative evaluation of relative spatiotemporal *ECa* patterns.

Two different procedures were applied to the filtered datasets, and all coil configurations were analysed separately. Mean subtraction (MS) was performed for each dataset and coil configuration by removing the mean *ECa* value calculated exclusively within the 9 × 6 m centred internal window, isolating intra-plot variability and suppressing seasonal variability linked to natural factors. Background subtraction (BS) was then conducted to assess long-term soil variability related to sub-soil treatments. The mean subtracted August 2016 dataset was assumed to represent the *ECa* background. The February 2019, October 2019, and October 2020 datasets were differenced point by point relative to this background, as all datasets had been interpolated onto the same grid, allowing discrimination between inherent soil heterogeneity and legacy effects of previous management and experimental interventions. The combined MS and BS procedures ($ECa^{MS\&BS}$) applied to the post-treatment datasets are formulated as follows:

$$ECa^{MS\&BS}_{x,s,2019Feb} = ECa_{x,s,2019Feb} - \overline{ECa_{s,2019Feb}} - (ECa_{x,s,2016Aug} - \overline{ECa_{s,2016Aug}}) \tag{4}$$

$$ECa^{MS\&BS}_{x,s,2019Oct} = ECa_{x,s,2019Oct} - \overline{ECa_{s,2019Oct}} - (ECa_{x,s,2016Aug} - \overline{ECa_{s,2016Aug}}) \tag{5}$$

$$ECa^{MS\&BS}_{x,s,2020Oct} = ECa_{x,s,2020Oct} - \overline{ECa_{s,2020Oct}} - (ECa_{x,s,2016Aug} - \overline{ECa_{s,2016Aug}}) \tag{6}$$

where $ECa_{x,s}$ represents the measured value at spatial position x for a specific coil configuration s, while the overbar denotes the spatial mean of the respective dataset. The date is specified for each *ECa* term to indicate the measurement period. In each equation, the first two terms constitute the MS, while the subsequent terms (representing the mean subtracted 2016 background) constitute the BS. For completeness and to avoid any possible misinterpretation, the equations are explicitly reported for each survey date. All processing steps were first applied to rectangles extracted from all plots across the entire field. The upper-left sector appeared more heterogeneous in all filtered *ECa* maps, whereas the lower-right sector showed more homogeneous patterns. Results were then evaluated over the entire area. Subsequently, datasets were reprocessed considering only rectangles corresponding to plots that exhibited the most homogeneous patterns on the *ECa* maps, primarily in the lower sector where the influence of subsoil manipulation was clearly observable. However, the initial heterogeneity observed in the upper-left sector had negligible impact on the final results. Therefore, for completeness and consistency, all plots across the entire field were retained in the final analysis.

2.5.2. EMI cropped field point-scale measurements and temporal trend analysis from may to august 2020

Point-scale measurements were processed using a relatively simplified workflow. For each coil configuration and for each point of measurement, *ECa* values recorded during the first and last five seconds of acquisition were removed to avoid potential operator-induced disturbances. The three timelapse datasets acquired at each measurement point along the south-eastern margin of each plot were then merged into a single dataset. Subsequently, datasets from plots that had undergone the same soil amelioration treatment (i.e., two plots per treatment) were grouped together. For each soil treatment and each coil configuration, the mean *ECa* value was then computed. To ensure comparability across all instrumentation settings, a normalization was applied to each coil configuration by subtracting the minimum measured average *ECa* value from all other mean values in each coil configuration. For each soil treatment, a linear line was fitted across the entire measurement period to characterize the *ECa* trend. In a next step, the slope of this regression was averaged across all coil configurations to provide a synthetic indicator of the temporal dynamics for each treatment. Furthermore, aggregate statistical metrics, including the mean, minimum, maximum, and variability were calculated for the different soil treatments by pooling the data from all coil configurations.

3. Results

3.1. Spatiotemporal ECa mapping and data processing performance

Measured *ECa* values across the CF2 experimental site ranged from approximately −5 to 20 mS/m throughout the four survey campaigns (August 2016, February 2019, October 2019, and October 2020), exhibiting clear spatial and temporal variability (Fig. 3). The generally higher *ECa* values observed during the August 2016 survey may partly reflect seasonal soil temperature effects, as no temperature correction was applied. However, because all subsequent analyses relied on coil-specific normalization procedures (MS and BS), any temperature-related offset was removed and did not affect the interpretation of relative spatiotemporal patterns. The VCP 0.32 m configuration consistently produced negative *ECa* values due to the absence of a site-specific calibration (von Hebel et al., 2019). Because the study focuses on relative spatiotemporal patterns and all subsequent normalization procedures were applied separately to each coil configuration, this offset did not affect data interpretation. However, the VCP 0.32 m configuration was excluded from further analyses because of its high signal variability associated with the shallow depth of investigation (von Hebel et al., 2019).

The August 2016 survey revealed pronounced spatial heterogeneity across the field, particularly in the deeper HCP configurations, where broad conductivity gradients and elongated conductive features were evident. Following the implementation of the subsoil treatments, the February 2019 survey showed the emergence of plot-scale *ECa* contrasts on top of the pre-existing spatial pattern. Subsequent surveys in October 2019 and October 2020 revealed the development of linear anomalies associated with the experimental layout, resulting in a more structured conductivity pattern across the field. Despite these temporal changes, several large-scale features observed in the 2016 background survey remained visible throughout the monitoring period, especially in the deeper HCP configurations. In addition, a localized conductivity anomaly was consistently detected in the upper part of the field across all survey dates and multiple coil configurations. Because this feature was already present in the pre-treatment survey and remained unchanged over time, it was considered unrelated to the experimental treatments and likely reflects an external source of electromagnetic interference.

Applying mean subtraction (MS) reduced the *ECa* variability range to approximately −5 to + 5 mS/m, thereby facilitating direct comparison among surveys acquired under different environmental conditions (Fig. 4). In the normalized August 2016 dataset, treatment plots were distributed across the full range of background *ECa* values, indicating that the randomized experimental design was not associated with any systematic conductivity pattern. In the post-treatment surveys, the large-scale spatial structures observed in the original background remained visible, particularly in the deeper configurations, demonstrating that normalization alone did not remove the persistent spatial heterogeneity of the site.

The BS procedure was subsequently applied to the MS datasets to remove the August 2016 background signal (Fig. 5). This correction substantially reduced the large-scale conductivity gradients that dominated the original maps, enhancing the visibility of treatment-related *ECa* contrasts. Compared with the MS datasets, the BS-corrected maps show a clearer delineation of plot-scale anomalies and a greater contrast between experimental plots and surrounding areas. Persistent linear features associated with the experimental layout remained visible throughout the monitoring period, together with a localized high-contrast anomaly present in all surveys and coil configurations.

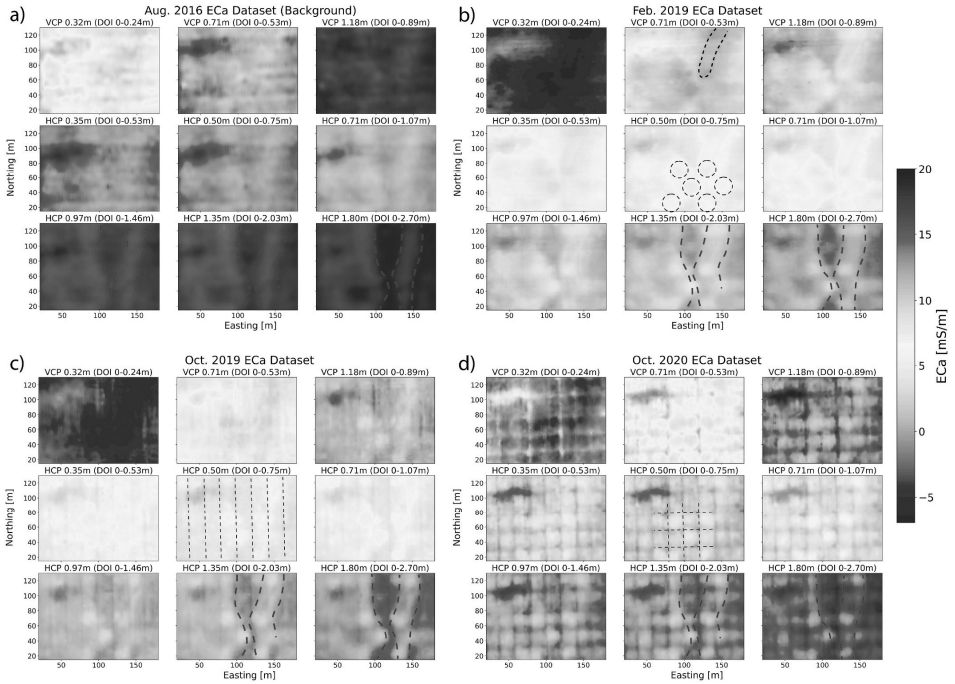


Fig. 3. Filtered and interpolated ECa maps for each field-scale acquisition from August 2016 to October 2020 for the three VCP configurations (0.32, 0.71, and 1.18 m) acquired with the CMD Mini-Explorer, and for the six HCP configurations (0.35, 0.50, 0.71, 0.97, 1.35, and 1.80 m) acquired with the CMD Mini-Explorer Special Edition. Dashed annotations highlight the principal spatial features discussed in the text, including persistent background conductive stripes (red), localized conductivity anomalies (black), and linear patterns associated with the experimental layout and traffic lanes (black).

Because this feature was already evident in the pre-treatment dataset and remained stable over time, it was considered unrelated to the experimental treatments and likely reflects external electromagnetic interference.

3.2. Theoretical signal contribution and treatment sensitivity

To contextualize the magnitude of the observed *ECa* patterns, the theoretical sensitivity of the EMI configurations (Eqs. (1) and (2)) was used to calculate the expected signal contribution originating from the 30–60 cm depth range (Eq. (3)), the specific soil layer where mechanical loosening and biowaste compost incorporation were performed. Table 1 details the specific DOI for each coil separation and configuration, and the percentage of the total signal originating from the 30–60 cm depth range.

The analysis reveals that the mechanical treatments influence only a fraction of the total signal, approximately 11.7 to 25.6% depending on the configuration. In contrast, the deep-rooting system of Lucerne, which can extend up to 3.7 m depth (Canadell et al., 1996), covers nearly 100% of the investigated sensitivity range (which reaches a maximum DOI of 2.7 m). Consequently, the biological influence is expected to exert a significantly stronger impact on the measured *ECa* compared to the localized mechanical modifications.

3.3. Statistical distribution of treatment effects across depths

To better quantify the impact of subsoil management on *ECa* distribution, MS- and BS-corrected *ECa* values were extracted from the 9 × 6 m internal plot areas and grouped according to treatment (Fig. 6). Treatment effects were evaluated using mixed linear models, with cover crop strategy (Ryegrass vs Lucerne) as a fixed effect and mechanical subsoil treatment (Control, DL, DLB) as a random effect. Overall, treatment differentiation increased with depth of investigation. At shallow depths, variability among treatments was limited, and mixed-model analysis indicated no significant differences between the Ryegrass and Lucerne groups ($p > 0.1$ for all survey dates). In contrast, intermediate and deeper investigation depths revealed a systematic separation between the two biological pre-conditioning strategies. Across the February 2019, October 2019, and October 2020 surveys, Ryegrass plots consistently exhibited significantly higher *ECa* values than Lucerne plots ($p < 0.001$ in all cases), demonstrating the robustness of this trend through time. Within the Lucerne treatments, a characteristic tendency toward higher *ECa* values was observed in DL.luc compared with both Control.luc and DLB.luc, whereas compost addition partially compensated for this increase. These differences persisted throughout the monitoring period, although they were not always statistically significant. In contrast, the Ryegrass treatments showed limited differentiation and little apparent sensitivity to mechanical intervention, maintaining comparatively higher and more uniform *ECa*

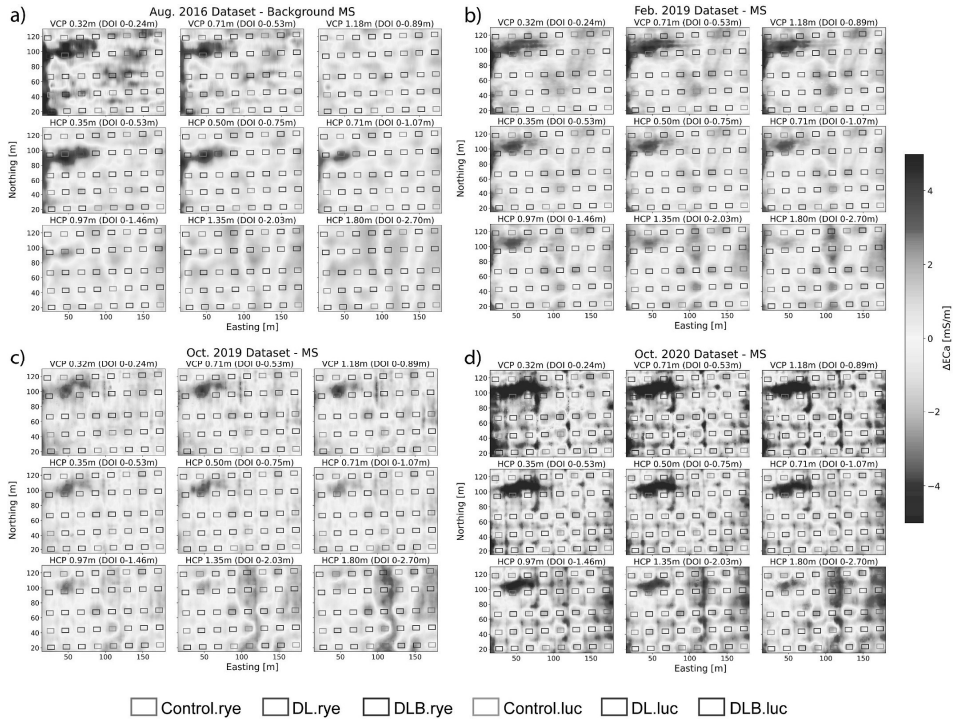


Fig. 4. ECa maps for the August 2016, February 2019, October 2019, and October 2020 datasets normalized by subtracting the mean subtraction (MS) calculated within the centred internal window, centred on the different treatment plots.

values. Overall, the results indicate that biological pre-conditioning exerted the strongest influence on *ECa* variability, while the effects of mechanical subsoil management were secondary and mainly expressed within the Lucerne series.

3.4. Intra-seasonal monitoring and soil treatment effects

The EMI point-scale measurements acquired during the 2020 growing season are presented in Fig. 7. Across all treatments, *ECa* values showed a progressive decline from May to late June, followed by a stabilization phase beginning around day 60. Short-term increases in *ECa* were associated with major precipitation events, indicating a clear influence of rainfall on the temporal dynamics of the signal. A consistent separation between the two biological pre-conditioning strategies was observed throughout the monitoring period. Plots previously cultivated with Lucerne maintained lower *ECa* values than Ryegrass plots across all measurement dates, confirming the spatial patterns identified in the field-scale surveys. As summarized in Table 2, mean *ECa* values ranged from 1.12 to 1.99 mS/m in the Lucerne treatments and from 2.24 to 2.92 mS/m in the Ryegrass treatments. Overall, the temporal monitoring confirms that biological pre-conditioning exerted a persistent influence on *ECa* dynamics throughout the growing season.

Regarding the drying rates, the Lucerne treatments subjected to mechanical intervention exhibited the most stable *ECa* dynamics, characterized by the lowest slope averages (−0.026), while the Ryegrass reference plots recorded the most rapid *ECa* declines, with slope averages of −0.033. The *ECa* signal in the Control.luc and Control.rye plots showed higher temporal variability (2.94 and 2.72 mS/m, respectively) compared to the deep loosening treatments, which displayed more stable and uniform electrical responses throughout the monitoring period, from 2.39 mS/m for the DL.luc to 2.68 mS/m for the DLB.rye.

3.5. Soil texture, bulk density, and hydraulic property analysis

Particle-size analysis confirmed the overall pedological uniformity of the Campus Klein Altendorf site, which is characterized by a silt-dominated loess-derived Haplic Luvisol (IUSS Working Group WRB, 2015) (Fig. A1). Consistent with this observation, the physical and hydraulic measurements showed limited differentiation among treatments at the pedon scale (Figs. A2 and A3). No substantial differences in bulk density or plant-available water were detected between the biological pre-treatments, the mechanically ameliorated plots, and the reference treatment. Most samples exhibited bulk density values of approximately 1.5 g cm^{-3}, consistent with the compacted Bt horizon described by Barej et al. (2014) and Kautz et al. (2013b). The only marked deviations were observed in the DLB.luc-B and DLB.rye-B samples, which showed substantially lower bulk density (0.6–0.9 g cm^{-3}) and altered water-retention characteristics. These samples were collected directly within the compost-amended slots and therefore represent localized conditions rather than the surrounding field-scale soil matrix.

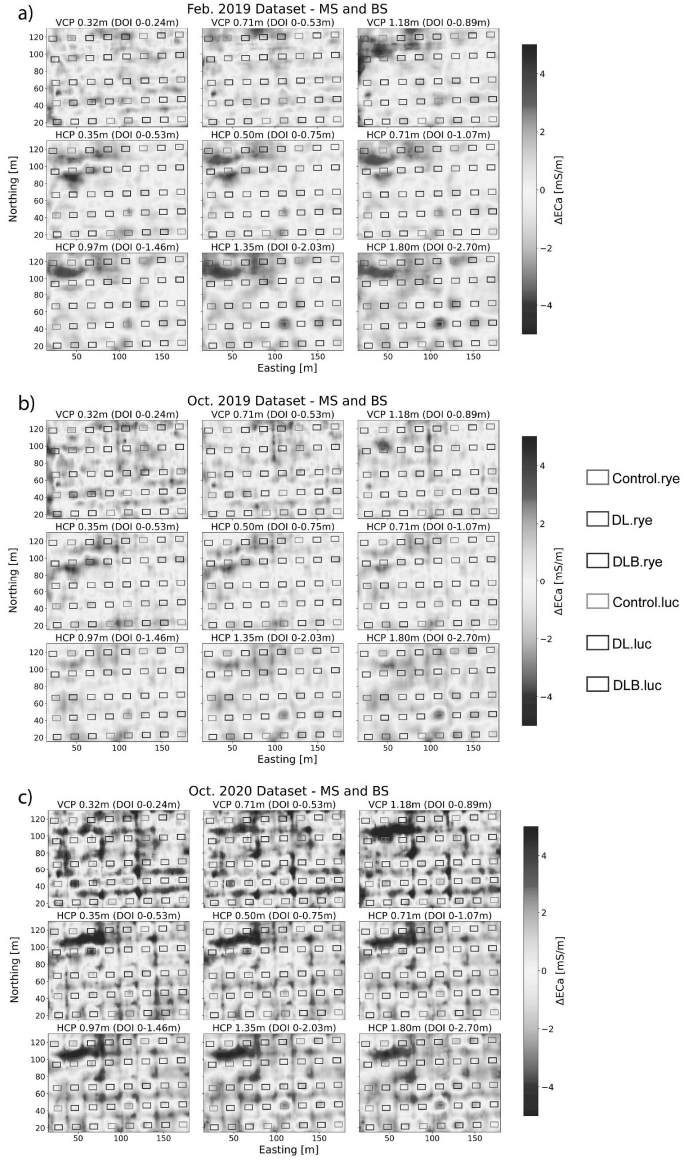


Fig. 5. ECa maps for the February 2019, October 2019, and October 2020 datasets obtained through the data-processing workflow developed in this study. For each coil configuration, all datasets were normalized by subtracting the mean subtraction (MS) calculated within the shown central rectangular areas. Subsequently, the mean subtracted August 2016 (background) dataset, was subtracted from the three datasets.

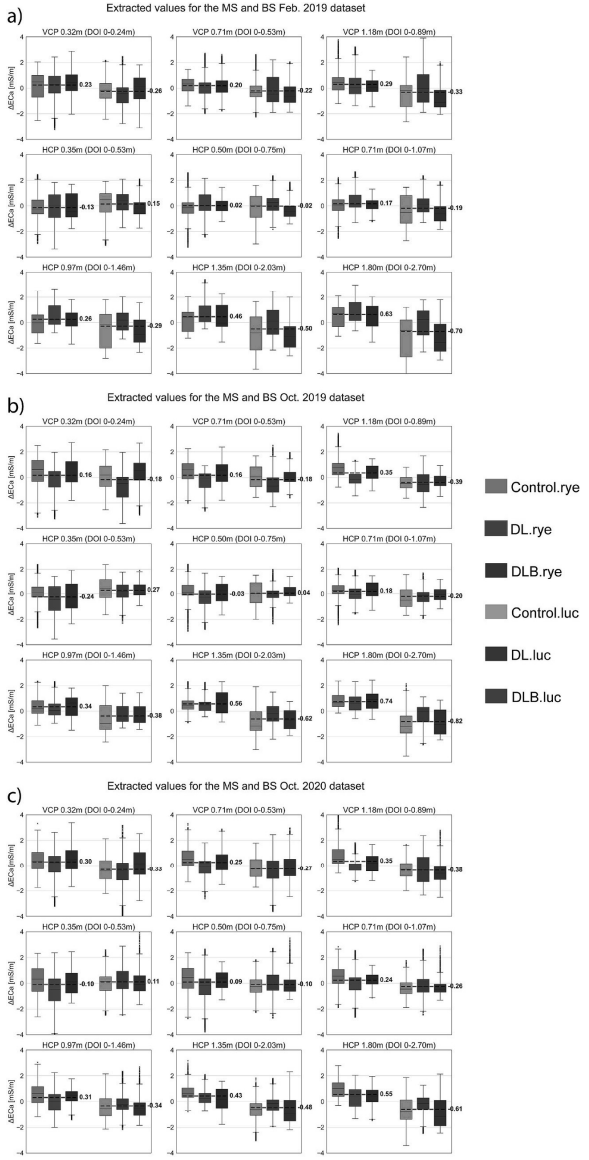


Fig. 6. Boxplots of ΔECa values extracted from the rectangular sampling areas for all coil configurations for the mean subtraction (MS) and background subtraction (BS) February 2019, October 2019, and October 2020 datasets. The boxplots illustrate the variability of soil ECa across the six management treatments (Control.rye, DL.rye, DLB.rye, Control.luc, DL.luc, DLB.luc). In the graphs, moving from left to right, increasing subsoil manipulations are observed (rye: Ryegrass cover crops; luc: Lucerne cover crops; Control: reference-control; DL: deep tillage; DLB: deep tillage with biowaste).

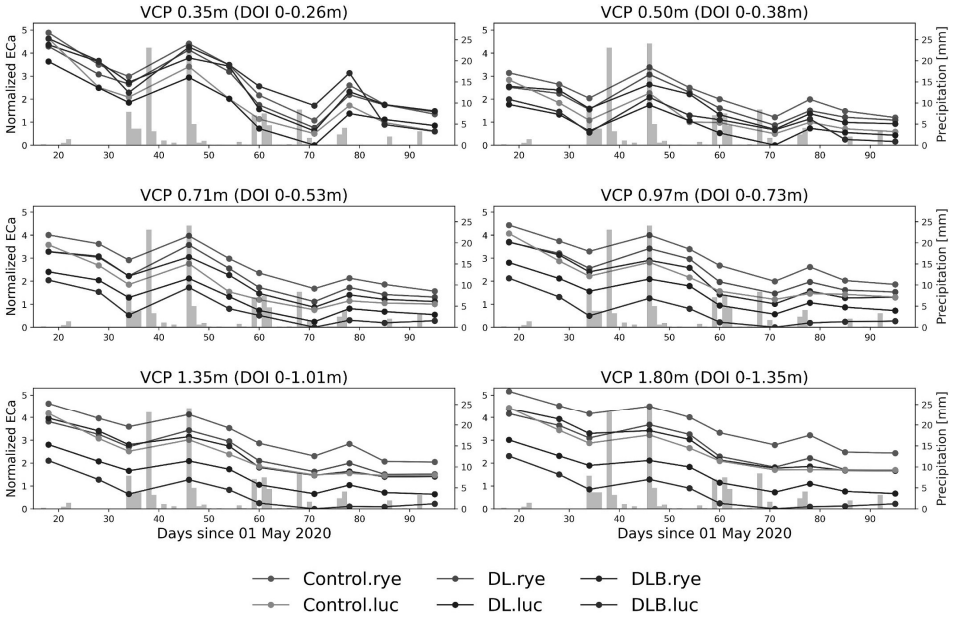


Fig. 7. Normalized mean ECa values derived from point-scale measurements collected in summer 2020 and grouped by soil treatment, as a function of the spring barley growth period for different VCP configurations (0.35, 0.50, 0.71, 0.97, 1.35, 1.80 m). Local measured precipitation (mm) is also reported in the graphs as blue histograms.

Table 2
Summary of ECa metrics and temporal dynamics for the different subsoil management treatments during the 2020 spring barley growing season. Values represent the mean of all coil configurations. ECa Slope Average indicates the rate of ECa decline per day [mS/m per day] derived from linear regression across the measurement period. Soil treatment abbreviations represent biological preconditioning (rye: Ryegrass; luc: Lucerne) and mechanical subsoil management (Control: reference-control; DL: deep loosening; DLB: deep loosening with biowaste compost incorporation).

Soil Treatment	*ECa* Average [mS/m]	*ECa* min [mS/m]	*ECa* max [mS/m]	*ECa* Variability [mS/m]	*ECa* Slope Average
Control.rye	2.92	1.70	4.42	2.72	−0.033
DL.rye	2.37	1.23	3.77	2.54	−0.029
DLB.rye	2.24	1.04	3.72	2.68	−0.033
Control.luc	1.99	1.02	3.96	2.94	−0.033
DL.luc	1.38	0.35	2.74	2.39	−0.026
DLB.luc	1.12	0.13	2.55	2.42	−0.026

4. Discussion

4.1. Natural soil variability, signal normalization and scale-dependent detection of management effects

Natural soil variability is a persistent challenge in both the interpretation of *ECa* measurements and in isolating management-induced effects. ECa spatial variability stems from soil texture variations (Abdu et al., 2017), parent material (Saey et al., 2013), and plant-related factors (e.g., root water extraction (Moghadas et al., 2017)). Temporal variability, in contrast, is due to short-term soil moisture-driven fluctuations and persistent patterns controlled by inherent soil properties. The latter constitute the stationary component of "soil memory", which is the soil's capacity to retain lasting imprints of inherent properties and past environmental states (Rahmati et al., 2023) over long temporal autocorrelation scales (Rahmati et al., 2024). Soil memory can effectively mask more subtle or transient signatures induced by management interventions. This masking was apparent in the August 2016 background EMI survey (Fig. 3a): even though the experimental site was initially selected for its presumed soil homogeneity, EMI revealed pre-existing spatial heterogeneity, particularly at greater depths (HCP 0.71–1.80 m). The two-step MS and subsequent BS correction (Eq. 4–6) was therefore essential to isolate subtle management-induced signatures not apparent in measured *ECa* values. The 9 × 6 m centred internal window was also critical as it excluded the substantial anthropogenic noise (~+3 mS/m) generated by machinery-induced compaction in the inter-plot corridors, ensuring that the analysis reflected only internal plot dynamics. While MS successfully normalized seasonal soil water content fluctuations, it did not remove the persistent spatial patterns linked to inherent soil structural and hydrological heterogeneity (Fig. 3a), which remained remarkably stable throughout the four-year monitoring period (Fig. 3b-d). Only the combined MS-BS application neutralized this pedological "soil memory" effectively. This allowed robust temporal comparisons of *ECa* maps that would otherwise have been significantly masked by the dominant natural soil background. The importance of the MS-BS correction becomes evident if the scale at which EMI detects soil properties and management effects is considered.

Laboratory analyses confirmed the overall pedological uniformity of the Campus Klein Altendorf site (Fig. A1), indicating that the observed spatial and temporal *ECa* patterns reflect management-induced structural and hydrological modifications rather than lithological contrasts alone. Despite this pedological uniformity, conventional soil core analyses (Fig. A2, A3) showed only minor differentiation between treatments in terms of bulk density and plant-available water, except for samples taken directly within compost-enriched slots. This discrepancy between EMI and laboratory measurements highlights a fundamental scale issue: point-scale sampling, such as small 250 cm^3 ring samples are unlikely to capture vertically connected biopores or heterogeneous and discontinuous strip-wise amelioration patterns (Arslan et al., 2026), thus likely missing localized structural modifications induced by subsoil amelioration management (Bauke et al., 2024).

From a geophysical perspective, EMI detected pronounced and spatially coherent *ECa* contrasts where laboratory metrics showed limited differentiation. This because EMI integrates both the soil matrix and the macropore network over meter-scale soil volumes, inherently capturing macroscopic heterogeneity, structural connectivity, and preferential flow pathways that are not resolved at the core scale (Schuh and Cline, 1990; Doolittle and Brevik, 2014). This does not imply that laboratory measurements are inaccurate. Cores characterize smaller components of the soil system, like soil matrix, whereas EMI likely reflects an integrated response of soil structure, soil water distribution, and root activity across the investigated depth interval. As a consequence, the pronounced field-scale *ECa* contrasts should be interpreted as macroscopic indicators of structural and hydrological reorganization rather than direct proxies of point-scale bulk density or water-retention parameters. EMI thus complements conventional analyses by bridging the gap between localized measurements and field-scale processes.

4.2. Structural legacies and their functional expression in crop water uptake

The term "soil memory" was used to refer to the natural, pedogenic background, primarily defined by inherent natural soil properties. Anthropogenic management practices that overlay this memory and reconfigure the subsoil architecture over multiple seasons (Rahmati et al., 2023) are instead defined as "structural legacies". The combined MS-BS correction demonstrates that the observed *ECa* patterns are not solely a pedogenic inheritance but also reflect more recent management-induced changes of the subsoil's stationary background. Beyond the inherent pedological heterogeneity revealed in the 2016 background survey (Fig. 3a), the BS-corrected datasets (Fig. 5) reveal two distinct anthropogenic signatures. First, traffic-related patterns, aligned with inter-plot corridors and persistent in the deepest-sensing EMI configuration (HCP 1.80 m), indicating structural modifications extending well below the plough layer. Second, biological preconditioning by Lucerne, which established a spatially coherent geoelectrical footprint that differed significantly from the Ryegrass control at deeper-sensing coil offsets (HCP 0.71–1.80 m) but not at shallower-sensing configurations (Fig. 6). This contrast persisted across the two-year monitoring period, despite mulching of pre-crops, mechanical interventions, and two cereal cropping cycles, indicating a durable subsoil modification. These findings are consistent with independent data from Arslan et al. (2026). The authors found that, at the same site, both pre-crops rooted to ≥ 200 cm but Lucerne developed significantly higher root length density below 60 cm, particularly at 130–165 cm, reflecting its deep taproot system and associated stable biopores that increase subsoil macroporosity (Uteau et al., 2013; Meurer et al., 2020). This form of bio-drilling likely explains the reduced *ECa* values observed in Lucerne-preconditioned plots. While enhanced macroporosity promotes infiltration and access to deep resources, it may also facilitate more efficient drainage and accelerate subsoil water depletion by subsequent crops (Gaiser et al., 2012). The resulting subsoil is structurally loosened yet hydraulically more dynamic and comparatively drier than the more compact and less permeable Ryegrass-preconditioned soil. The consistent offset toward lower *ECa* values in Lucerne plots was also observed throughout the 2020 growing season in the point-scale EMI monitoring (Fig. 7), suggesting that biological pre-conditioning enhanced access to deeper water reserves and reduced residual subsoil water contents. The progressive decline in *ECa*, followed by a more stable plateau, is consistent with the transition from active root water uptake to crop senescence. Here, the strong temporal variability shallow-sensing configurations (VCP 0.35–0.50 m) likely reflects sensitivity to near-surface soil moisture fluctuations. Smoother trends in deeper layers, instead, suggest that subsoil *ECa* dynamics were primarily governed by sustained root activity rather than transient precipitation events. The interpretation that biological legacies exerted a dominant control on subsoil functioning is reinforced by *ECa* patterns from VCP 0.71 and deeper sensing coils, which closely mirrored the field-scale treatment contrasts. This is further corroborated by the higher root length density following Lucerne found by Arslan et al. (2026) and by isotopic evidence of greater water uptake below 60 cm from Eitelberg et al. (under review). Overall, these findings suggest that the geoelectrical signal integrates structural modifications with enhanced exploitation of deep-water reserves, rather than reflecting solely physical changes in the soil matrix.

Biological pre-conditioning appeared to dominate over mechanical treatments in the integrated EMI response. This is largely because mechanical loosening interventions from 2018 were confined to the 30–60 cm depth interval, which contributes only 11.7–25.6% of the total EMI signal, depending on the coil configuration (McNeill, 1980; Table 1). Consequently, structural or hydrological modifications restricted to this depth range are inherently attenuated within the integrated EMI response. Despite this attenuation, interactions between biological and mechanical treatments were detectable. A characteristic dome-shaped pattern is apparent in the statistical distributions of Lucerne plots (Fig. 6). This was mainly driven by DL.luc treatment, which consistently exhibited higher mean *ECa* values than both Control.luc and DLB.luc, particularly in the deeper-sensitive HCP 1.35 and 1.80 configurations. Increased bulk density and reduced pore continuity following structural degradation are typically associated with higher *ECa* values. Thus, the observations are consistent with the negative impacts of mechanical deep loosening without organic amendment, which can result in rapid structural recovery and re-compaction of the loosened layer (Larney and Fortune, 1986; Eitelberg et al., under review), possibly leading to a denser and hydraulically less efficient subsoil over time. Conversely, the DLB.luc treatment shifted toward lower *ECa* values, approaching those of the reference Lucerne treatment and consistent with improved plant and root development following compost incorporation. Compost addition can significantly enhance the exploitation of deep-water reserves at the site, with 44.9% of total root water uptake below 60 cm compared with 35.9% under mechanical loosening alone (Eitelberg et al., under review). Similarly, more gradual *ECa* declines during the growing season suggest a more sustained water supply in DLB plots. Therefore, compost appears to create favourable conditions for root growth and deep resource acquisition on top of its ability to function as a passive water reservoir. This interpretation is further supported by the downward shift in nutrient uptake zones reported by Uhlig et al. (2023) and the increased maximum rooting depths observed by Bauke et al. (2024). Notably, these treatment-specific responses were confined to the Lucerne series whereas ryegrass plots consistently showed higher *ECa* values and negligible sensitivity to mechanical intervention, without recurring spatial or temporal treatment patterns (Figs. 6 and 7). This suggests that: a) the effectiveness of mechanical subsoil amelioration depends strongly on prior biological structuring and b) mechanical measures appear most effective when biopore networks and improved connectivity have already been established by biologically preconditioning. In the absence of such biological legacies, the impact of mechanical tillage on the integrated EMI signal, and likely on subsoil functioning, remains limited.

Overall, both field-scale and intra-seasonal EMI observations show a

clear treatment hierarchy in *ECa* response magnitude and in water-use dynamics, with DLB < DL < Control within the Lucerne series. Here, the EMI signal appears to integrate structural differences with hydrological and plant physiological processes operating within the soil-root continuum. This combined geophysical evidence thus indicates that biological pre-conditioning at the site establishes persistent structural legacies that improve access to deep soil water reserves, while mechanical-organic amelioration can further enhance their functionality.

4.3. Implications, limitations, and outlook for long-term subsoil experiments

This study shows that geophysical diagnostics should be integrated into the design and monitoring of long-term subsoil experiments. The pronounced spatial heterogeneity detected by the baseline EMI survey at a site initially considered homogeneous highlights the risk that latent pedological gradients may unintentionally coincide with treatment allocation, thereby masking management effects. Pre-treatment EMI mapping thus provides a non-invasive complement to point-scale investigations. The combination with MS and BS further strengthens the framework, allowing the separation of management-induced signals from the natural soil background and the tracking of the persistence of anthropogenic structural legacies over time.

Nonetheless, some limitations of the study and of the EMI method should be acknowledged. The interpretation of geoelectrical patterns remains challenging because *ECa* integrates structural, hydrological, and biological processes. Without a site-specific calibration, *ECa* cannot generally be converted into absolute volumetric soil water content, restricting interpretations to relative dynamics. Moreover, although the observed *ECa* patterns are consistent with known rooting behaviour, the current experimental design does not allow complete separation of structural effects (biopore connectivity) from functional effects (root water uptake). Complementary information on plant development and soil water dynamics would have been helpful but was not available in this study.

Future research should therefore focus on multi-sensor approaches that strengthen the quantitative interpretation of EMI data. For example, site-specific calibration via electrical resistivity tomography (ERT) could facilitate the conversion of relative *ECa* patterns into absolute conductivity estimates, while ground-penetrating radar (GPR) may provide complementary information on subsoil architecture and soil water distribution. Combined with direct soil water measurements and plant observations, these geophysical methods would strengthen attribution of management-induced variability and improve assessment of long-term subsoil functioning.

5. Conclusions

This study demonstrates that multi-coil EMI is a powerful and scalable tool for assessing the structural and functional legacies of biological and mechanical subsoil management. By integrating electrical responses over meter-scale volumes, EMI could detect macroscopic changes in soil architecture and biopore connectivity that might be missed by traditional, small-volume soil sampling. A primary finding is the significant pre-existing pedological heterogeneity site, alongside the persistent anthropogenic structural legacies from machinery traffic revealed even at larger soil depths. The long-term detectability of these management-induced imprints confirms their role in reconfiguring the soil's memory over multiple seasons. This underscores, that high-resolution EMI premapping should be considered a fundamental diagnostic tool for experimental design, allowing for "smart" plot allocation that accounts for inherent soil variability and prevents pedological "noise" from confounding treatment effects. In this context, the combined mean subtraction (MS) and background subtraction (BS) workflow proved essential to decouple the inherent pedological background (i.e., the signatures of the unmanaged soil) from the management-induced signals. Our results suggest that biological pre-conditioning with Lucerne induces a vertically integrated and durable "reprogramming" of the subsoil, consistent with enhanced macroporosity and deeper, more efficient water extraction by subsequent crops. In contrast, mechanical loosening appears more localized and attenuated, likely due to its limited volumetric footprint. However, the modulation of *ECa* patterns by biowaste compost incorporation suggests that organic amendments may act as a catalyst for root vigour, supporting a more sustained water supply during the growing season. Time-lapse EMI monitoring provides a non-invasive framework to quantify the depth and persistence of subsoil amelioration. By bridging the gap between localized matrix measurements and field-scale functioning, this approach represents a key methodological advancement for evaluating sustainable management strategies and improving crop resource use efficiency under real cropping conditions.

CRediT authorship contribution statement

Aaron Sobbe: Writing – review & editing, Writing – original draft, Visualization, Software, Methodology, Investigation, Formal analysis. **Jessica Schmäck:** Writing – review & editing, Writing – original draft, Methodology, Investigation, Formal analysis. **Cosimo Brogi:** Writing – review & editing, Writing – original draft, Visualization, Validation, Software. **Anja Klotzsche:** Writing – review & editing, Validation, Supervision, Software, Project administration, Methodology, Investigation, Formal analysis, Conceptualization. **Lutz Weihermüller:** Writing – review & editing, Validation. **Harry Vereecken:** Writing – review & editing, Validation. **Enzo Rizzo:** Writing – review & editing, Supervision. **Jan van der Kruk:** Writing – review & editing, Writing – original draft, Visualization, Validation, Supervision, Software, Methodology, Investigation, Funding acquisition, Conceptualization.

Declaration of competing interest

The authors declare that they have no known competing financial interests or personal relationships that could have appeared to influence the work reported in this paper.

Acknowledgements

This work was supported by the German Federal Ministry of Education and Research (BMBF) in the framework of the funding measure 'Soil as a Sustainable Resource for the Bioeconomy - BonaRes', project 'BonaRes (Module A): Sustainable Subsoil Management - Soil3- II; subproject C' (grant number 031B0515C). The authors also acknowledge the support of the PhenoRob - Cluster of Excellence in Robotics and Phenotyping for Sustainable Crop Production, funded by the Deutsche Forschungsgemeinschaft (DFG, German Research Foundation) under Germany's Excellence Strategy (EXC 2070 – 390732324), in which the University of Bonn and Forschungszentrum Jülich participate. The authors would like to thank Manuela Kaufmann, Christian von Hebel, Tobias Ganther, Yi Yu, Sebastian Singer, Shirin Bagheri, Nicole Höring, Lena Lärm, and Sören Netz for their invaluable assistance during field data acquisition, as well as Anke Langen and Lutz Weihermüller for their support with laboratory activities within the Soil^3 project.

Appendix A. Supplementary data

Supplementary data to this article can be found online at https://doi.org/10.1016/j.geoderma.2026.118001.

Data availability

Data will be made available on request.

References

Abdu, H., Robinson, D.A., Boettinger, J., Jones, S.B., 2017. Electromagnetic induction mapping at varied soil moisture reveals field-scale soil textural patterns and gravel lenses. Front. Agric. Sci. Eng. 4 (2), 135–145.
Amelung, W., Bossio, D., de Vries, W., Kögel-Knabner, I., Lehmann, J., Amundson, R., Chabbi, A., 2020. Towards a global-scale soil climate mitigation strategy. Nat. Commun. 11 (1), 5427.
Arslan, M., Kemper, R., Döring, T.F., Schmittmann, O., Athmann, M., 2026. Effects of biological and technical subsoil amelioration on root growth and crop performance in cereal crops. Soil Tillage Res. 256, 106907.
Barej, J.A.M., Pätzold, S., Perkons, U., Amelung, W., 2014. Phosphorus fractions in bulk subsoil and its biopore systems. Eur. J. Soil Sci. 65 (4), 553–561.
Bauke, S.L., Seidel, S.J., Athmann, M., Berns, A.E., Braun, M., Gocke, M.I., Amelung, W., 2024. Short-term effects of subsoil management by strip-wise loosening and incorporation of organic material. Soil Tillage Res. 236, 105936.
Berg, A., Sheffield, J., 2018. Climate change and drought: the soil moisture perspective. Current Climate Change Reports 4 (2), 180–191.
Binley, A., Hubbard, S.S., Huisman, J.A., Revil, A., Robinson, D.A., Singha, K., Slater, L. D., 2015. The emergence of hydrogeophysics for improved understanding of subsurface processes over multiple scales. Water Resour. Res. 51 (6), 3837–3866.
Brogi, C., Huisman, J.A., Pätzold, S., von Hebel, C., Weihermüller, L., Kaufmann, M.S., van der Kruk, J., Vereecken, H., 2019. Large-scale soil mapping using multi-configuration EMI and supervised image classification. Geoderma 335, 133–148.
Brogi, C., Huisman, J.A., Herbst, M., Weihermüller, L., Klosterhalfen, A., Montzka, C., Reichenau, T.G., Vereecken, H., 2020. Simulation of spatial variability in crop leaf area index and yield using agroecosystem modeling and geophysics-based quantitative soil information. Vadose Zone J. 19 (1), e20009.
Brogi, C., Huisman, J.A., Weihermüller, L., Herbst, M., Vereecken, H., 2021. Added value of geophysics-based soil mapping in agro-ecosystem simulations. Soil 7, 125–143.
Brown, M., Heinse, R., Johnson-Maynard, J., Huggins, D., 2021. Time-lapse mapping of crop and tillage interactions with soil water using electromagnetic induction. Vadose Zone J. 20 (4), e20097.
Canadell, J., Jackson, R.B., Ehleringer, J.B., Mooney, H.A., Sala, O.E., Schulze, E.D., 1996. Maximum rooting depth of vegetation types at the global scale. Oecologia 108 (4), 583–595.
Cassiani, G., Boaga, J., Vanella, D., Perri, M.T., Consoli, S., 2015. Monitoring and modelling of soil-plant interactions: the joint use of ERT, sap flow and eddy covariance data to characterize the volume of an orange tree root zone. Hydrol. Earth Syst. Sci. 19 (5), 2213–2225.
Cimpoiașu, M.O., Kuras, O., Pridmore, T., Mooney, S.J., 2020. Potential of geoelectrical methods to monitor root zone processes and structure: a review. Geoderma 365, 114232.
Corwin, D.L., Lesch, S.M., 2005. Apparent soil electrical conductivity measurements in agriculture. Comput. Electron. Agric. 46 (1–3), 11–43.
Dogar, S.S., Brogi, C., O'Leary, D., Hernández-Ochoa, I.M., Donat, M., Vereecken, H., Huisman, J.A., 2025. Combining electromagnetic induction and satellite-based NDVI data for improved determination of management zones for sustainable crop production. Soil 11 (2), 655–679.
Doolittle, J.A., Brevik, E.C., 2014. The use of electromagnetic induction techniques in soils studies. Geoderma 223, 33–45.
Eitelberg, L., Sun, Y., Amelung, W., Rothfuss, Y., Schmittmann, O., Bauke, S.L., under review. Subsoil amelioration strategies and their effect on crop water use and water use efficiency. Manuscript under review for publication in Soil & Tillage Research.
Frederiksen, R.R., Christiansen, A.V., Christensen, S., Rasmussen, K.R., 2017. A direct comparison of EMI data and borehole data on a 1000 ha data set. Geoderma 303, 188–195.
Gaiser, T., Perkons, U., Küpper, P.M., Puschmann, D.U., Peth, S., Kautz, T., Köpke, U., 2012. Evidence of improved water uptake from subsoil by spring wheat following lucerne in a temperate humid climate. Field Crop Res 126, 56–62.
Garré, S., Hyndman, D., Mary, B., Werban, U., 2021. Geophysics conquering new territories: the rise of "agrogeophysics". Vadose Zone J. 20 (4), e20115.
Gocke, M.I., Don, A., Heidkamp, A., Schneider, F., Amelung, W., 2021. The phosphorus status of German cropland - an inventory of top- and subsoils. J. Plant Nutr. Soil Sci. 184, 51–64.
Grote, K., Anger, C., Kelly, B., Hubbard, S., Rubin, Y., 2010. Characterization of soil water content variability and soil texture using GPR groundwave techniques. J. Environ. Eng. Geophys. 15 (3), 93–110.
Hamza, M.A., Anderson, W.K., 2005. Soil compaction in cropping systems: a review of the nature, causes and possible solutions. Soil Tillage Res. 82 (2), 121–145.
Han, E., Kautz, T., Perkons, U., Uteau, D., Peth, S., Huang, N., Köpke, U., 2015. Root growth dynamics inside and outside of soil biopores as affected by crop sequence determined with the profile wall method. Biol. Fertil. Soils 51 (7), 847–856.
Heil, K., Schmidhalter, U., 2017. The application of EM38: Determination of soil parameters, selection of soil sampling points and use in agriculture and archaeology. Sensors 17 (11), 2540.
IUSS Working Group WRB, 2015. World reference base for soil resources 2014, update 2015, International soil classification system for naming soils and creating legends for soil maps. World Soil Resources Report 106. Rome, Italy: Food and Agriculture Organization of the United Nations.
Johnson, C.K., Eigenberg, R.A., Doran, J.W., Wienhold, B.J., Eghball, B., Woodbury, B.L., 2005. Status of soil electrical conductivity studies by central state researchers. Trans. ASAE 48 (3), 979–989.
Jung, W.K., Kitchen, N.R., Sudduth, K.A., Kremer, R.J., Motavalli, P.P., 2005. Relationship of apparent soil electrical conductivity to claypan soil properties. Soil Sci. Soc. Am. J. 69 (3), 883–892.
Kaufmann, M.S., Klotzsche, A., Vereecken, H., van Der Kruk, J., 2020a. Simultaneous multichannel multi-offset ground-penetrating radar measurements for soil characterization. Vadose Zone J. 19 (1), e20017.
Kaufmann, M.S., von Hebel, C., Weihermüller, L., Baumecker, M., Döring, T., Schweitzer, K., van Der Kruk, J., 2020b. Effect of fertilizers and irrigation on multi-configuration electromagnetic induction measurements. Soil Use Manag. 36 (1), 104–116.
Kaufmann, M.S., Klotzsche, A., van der Kruk, J., Langen, A., Vereecken, H., Weihermüller, L., 2025. Assessing soil fertilization effects using time-lapse electromagnetic induction. Soil 11 (1), 267–285.
Kautz, T., Amelung, W., Ewert, F., Gaiser, T., Horn, R., Jahn, R., Köpke, U., 2013a. Nutrient acquisition from arable subsoils in temperate climates: a review. Soil Biol. Biochem. 57, 1003–1022.
Kautz, T., Perkons, U., Athmann, M., Pude, R., Köpke, U., 2013b. Barley roots are not constrained to large-sized biopores in the subsoil of a deep Haplic Luvisol. Biol. Fertil. Soils 49 (7), 959–963.
Keller, G.V., Frischknecht, F.C., 1966. Electrical methods in geophysical prospecting.
Keller, T., Lamandé, M., Peth, S., Berli, M., Delenne, J.Y., Baumgarten, W., Or, D., 2013. An interdisciplinary approach towards improved understanding of soil deformation during compaction. Soil Tillage Res. 128, 61–80.
Kirkegaard, J.A., Lilley, J.M., Howe, G.N., Graham, J.M., 2007. Impact of subsoil water use on wheat yield. Aust. J. Agr. Res. 58 (4), 303–315.
Larney, F.J., Fortune, R.A., 1986. Recompaction effects of mouldboard ploughing and seedbed cultivations on four deep loosened soils. Soil Tillage Res. 8, 77–87.
Martini, E., Werban, U., Zacharias, S., Pohle, M., Dietrich, P., Wollschläger, U., 2017. Repeated electromagnetic induction measurements for mapping soil moisture at the field scale: Validation with data from a wireless soil moisture monitoring network. Hydrol. Earth Syst. Sci. 21 (1), 495–513.
McNeill, J.D., 1980. Electromagnetic terrain conductivity measurement at low induction numbers. Geonics Limited Ontario, Canada.
Meurer, K., Barron, J., Chenu, C., Coucheney, E., Fielding, M., Hallett, P., Jarvis, N., 2020. A framework for modelling soil structure dynamics induced by biological activity. Glob. Chang. Biol. 26 (10), 5382–5403.
Moghadas, D., Jadoon, K.Z., McCabe, M.F., 2017. Spatiotemporal monitoring of soil water content profiles in an irrigated field using probabilistic inversion of time-lapse EMI data. Adv. Water Resour. 110, 238–248.
Ni, J.J., Cheng, Y.F., Bordoloi, S., Bora, H., Wang, Q.H., Ng, C.W.W., Garg, A., 2019. Investigating plant root effects on soil electrical conductivity: an integrated field monitoring and statistical modelling approach. Earth Surf. Proc. Land. 44 (3), 825–839.
Ning, T., Liu, Z., Hu, H., Li, G., Kuzyakov, Y., 2022. Physical, chemical and biological subsoiling for sustainable agriculture. Soil Tillage Res. 223, 105490.
Passioura, J.B., 2002. Soil conditions and plant growth. Plant Cell Environ. 25 (2), 311–318.
Quiros-Vargas, J., Brogi, C., Damm, A., Siegmann, B., Rademske, P., Burchard-Levine, V., Krieger, V., Schmidt, M., Hanuš, J., Martello, M., Weihermüller, L., Muller, O., Rascher, U., 2026. Solar-induced chlorophyll fluorescence (SIF) tracks variations in the soil-plant available water (PAW): a multiyear analysis on three crops. Sci. Remote Sens. 13, 100367.
Rahmati, M., Or, D., Amelung, W., Bauke, S.L., Bol, R., Hendricks Franssen, H.J., Vereecken, H., 2023. Soil is a living archive of the Earth system. Nat. Rev. Earth Environ. 4 (7), 421–423.
Rahmati, M., Amelung, W., Brogi, C., Dari, J., Flammini, A., Bogena, H., Vereecken, H., 2024. Soil moisture memory: State-of-the-art and the way forward. Rev. Geophys. 62 (2), e2023RG000828.
Robinson, D.A., Campbell, C.S., Hopmans, J.W., Hornbuckle, B.K., Jones, S.B., Knight, R., Wendroth, O., 2008. Soil moisture measurement for ecological and hydrological watershed-scale observatories: a review. Vadose Zone J. 7 (1), 358–389.
Romero-Ruiz, A., Linde, N., Keller, T., Or, D., 2018. A review of geophysical methods for soil structure characterization. Rev. Geophys. 56 (4), 672–697.
Rumpel, C., Chabbi, A., Marschner, B., 2012. Carbon storage and sequestration in subsoil horizons: knowledge, gaps and potentials. In: Recarbonization of the Biosphere: Ecosystems and the Global Carbon Cycle. Springer Netherlands, Dordrecht, pp. 445–464.
Saey, T., De Smedt, P., De Clercq, W., Meerschman, E., Monirul Islam, M., Van Meirvenne, M., 2013. Identifying soil patterns at different spatial scales with a multi-receiver EMI sensor. Soil Sci. Soc. Am. J. 77 (2), 382–390.
Schmäck, J., Weihermüller, L., Klotzsche, A., von Hebel, C., Pätzold, S., Welp, G., Vereecken, H., 2022. Large-scale detection and quantification of harmful soil compaction in a post-mining landscape using multi-configuration electromagnetic induction. Soil Use Manag. 38 (1), 212–228.
Schmittmann, O., Christ, A., Schulze Lammers, P., 2021. Subsoil melioration with organic material-principle, technology and yield effects. Agronomy 11 (10), 1970.
Schneider, F., Don, A., 2019. Root-restricting layers in German agricultural soils. Part I: extent and cause. Plant and Soil 442 (1), 433–451.
Schuh, W.M., Cline, R.L., 1990. Effect of soil properties on unsaturated hydraulic conductivity pore-interaction factors. Soil Sci. Soc. Am. J. 54 (6), 1509–1519.
Seidel, S.J., Gaiser, T., Kautz, T., Bauke, S.L., Amelung, W., Barfus, K., Athmann, M., 2019. Estimation of the impact of precrops and climate variability on soil depth-differentiated spring wheat growth and water, nitrogen and phosphorus uptake. Soil Tillage Res. 195, 104427.
Sobbe, A., Brombin, V., Rizzo, E., Bianchini, G., 2025. Saline peatland degradation in the Mezzano lowland: 66 years of agricultural impacts on carbon and soil biogeochemistry. Land 14 (8), 1621.

Stadler, A., Rudolph, S., Kupisch, M., Langensiepen, M., van der Kruk, J., Ewert, F., 2015. Quantifying the effects of soil variability on crop growth using apparent soil electrical conductivity measurements. Eur. J. Agron. 64, 8–20.
Uhlig, D., Berns, A.E., Wu, B., Amelung, W., 2023. Mean nutrient uptake depths of cereal crops change with compost incorporation into subsoil-evidence from 87Sr/86Sr ratios. Plant and Soil 489 (1), 613–628.
Uteau, D., Pagenkemper, S.K., Peth, S., Horn, R., 2013. Root and time dependent soil structure formation and its influence on gas transport in the subsoil. Soil Tillage Res. 132, 69–76.
Vereecken, H., Schnepf, A., Hopmans, J.W., Javaux, M., Or, D., Roose, T., Young, I.M., 2016. Modelling soil processes: Review, key challenges, and new perspectives. Vadose Zone J. 15 (5), vzj2015-09.
Von Hebel, C., Rudolph, S., Mester, A., Huisman, J.A., Kumbhar, P., Vereecken, H., van der Kruk, J., 2014. Three-dimensional imaging of subsurface structural patterns using quantitative large-scale multiconfiguration electromagnetic induction data. Water Resour. Res. 50 (3), 2732–2748.
Von Hebel, C., Matveeva, M., Verweij, E., Rademske, P., Kaufmann, M.S., Brogi, C., van der Kruk, J., 2018. Understanding soil and plant interaction by combining ground-based quantitative electromagnetic induction and airborne hyperspectral data. Geophys. Res. Lett. 45 (15), 7571–7579.
Von Hebel, C., Van der Kruk, J., Huisman, J.A., Mester, A., Altdorff, D., Endres, A.L., Vereecken, H., 2019. Calibration, conversion, and quantitative multi-layer inversion of multi-coil rigid-boom electromagnetic induction data. Sensors 19 (21), 4753.
Ward, S.H., Hohmann, G.W., 1987. Electromagnetic theory for geophysical applications.